JICE Journal Innovation of Civil Engineering

Vol. 6, No. 2, pp. 170-193
Submit: 04-07-2025 |
Accepted: 29-12-2025 |
Publish: 31-12-2025 |

The Design and Assessment of the Hollow Precast Wall with Integrated Active Ventilation System, for Minimizing Heat Retention, Removing Heat Load

Kongphat Phaiboonnukulkij
Faculty of Architecture, 254 Phaya Thai Rd, Wang Mai, Pathum Wan, Bangkok, 10330, Thailand

e-mail: 6778001525@student.chula.ac.th

ABSTRACT
Cooling demand in hot, humid climates is driven primarily by heat gains through the building envelope, particularly through opaque wall elements. Conventional static insulation systems reduce steady-state heat transfer but are limited in their ability to dissipate stored heat and respond dynamically to transient thermal loads. This study presents a comprehensive assessment of an actively ventilated hollow precast wall system designed to enhance heat removal through low-speed forced airflow within an internal cavity. A coupled analytical and numerical methodology is employed to quantify airflow-dependent thermal resistance, heat flux reduction, and transient thermal response under conditions representative of hot climates. The results demonstrate that introducing very low airflow (approximately 0.1 m/s) increases the effective thermal resistance by about 28% and reduces heat transfer by more than 50% compared with a non-ventilated wall. The most significant performance improvement occurs during the transition from natural to weak forced convection, while higher airflow rates yield diminishing returns. The findings indicate that actively ventilated hollow precast walls can function as low-energy, hybrid passive–active envelope systems with strong potential to reduce cooling loads in tropical and subtropical buildings.

Keywords: *Actively ventilated wall; Hollow precast wall; Dynamic insulation; Thermal resistance; Building envelope energy performance.*

1. Introduction

The research on the hollow precast wall focuses on a design that integrates an air blower system at the base of the panel. This system introduces cool air into the hollow core of the wall, which is then forced upward through the panel's chambers. As the air moves through, it absorbs and removes excess heat, expelling it through strategically placed exhaust holes at the top of the panel. This continuous airflow actively manages heat retention and enhances the wall's thermal mass [53]. Inspired by the Ventilated Hollow Core Slab (VHCS) system, this wall panel is designed to address heat load removal in building structures, providing a more efficient thermal mass solution than traditional systems [16]. By utilizing forced air movement, the panel rapidly dissipates heat that accumulates in its hollow core, improving energy performance and helping maintain indoor thermal comfort [13].

This design is particularly advantageous in hot climates, where passive cooling techniques are essential to reduce dependence on mechanical HVAC systems [51]. The hollow precast wall is engineered to reduce peak thermal loads significantly. The system actively channels cool air through the hollow core, minimizing heat retention and optimizing the wall's thermal mass performance [33]. This not only lowers the wall's internal temperature but also reduces strain on mechanical cooling systems by lessening the building's peak thermal load. As a result, it contributes to energy efficiency by reducing air conditioning demand while maintaining stable indoor temperatures during the hottest

Vol. 6, No. 2, pp. 170-193
Submit: 04-07-2025 |
Accepted: 29-12-2025 |
Publish: 31-12-2025 |

parts of the day. The continuous airflow within the wall ensures rapid heat dissipation, preventing heat buildup and effectively managing peak loads [64]. This system offers greater thermal regulation, particularly in high-temperature environments, making it a highly effective passive-cooling solution for energy-efficient building designs.

Sandwich panels are widely used in prefabricated buildings due to their cost-effectiveness, rapid installation, and strong thermal insulation. They typically consist of an insulating core between coated galvanized steel sheets and offer advantages in maintenance, dismantling, and heat retention. However, increasing demands for building energy efficiency and fire safety have driven the need for further improvements in their thermal and fire-resistant performance. Studies show the energy-saving potential of optimized insulation systems. Mohsen and Akash [4] reported that proper insulation can reduce building energy use by up to 77% and lower CO_2 emissions by 27%. Mahlia et al. [43] concluded that the optimal insulation thickness occurs when the additional material cost outweighs the energy-saving benefits. Other research identifies temperature, moisture, density, thickness, and airflow velocity as key determinants of insulation performance. Marani and Madhkhan [45] demonstrated that phase-change materials in concrete sandwich panels can reduce interior wall surface temperatures by 5.4°C. Lee and Pessiki [8] found that triple-layer concrete panels with staggered connections provide higher thermal resistance than double-layer panels. Additional findings include superior low-temperature performance of air-laid feather fiber insulation compared to elastomeric foam, and a 20% increase in heat flux through walls with joint defects, as observed by Nardi et al. [30]. Ochs et al. [48] emphasized that elevated moisture content significantly degrades insulation performance.

Research on fire resistance has also expanded. Pereira et al. found that cork-core sandwich panels with GFRP skins improve fire resistance, while Ma et al. [42] showed that ceramic concrete panels reinforced with alkali-resistant glass fibers achieve a 5% increase in fire resistance. Proença et al. [50] reported that adding calcium silicate boards enhances fire resistance by a factor of three to four.

Wind-induced pressure variations across building surfaces play a critical role in shaping ventilation patterns and thermal performance, especially in systems that integrate dynamic insulation or active wall technologies. As wind moves around a structure, external pressure fluctuates with wind speed, direction, building geometry, and site exposure. The equation describes this relationship:

$$P_\omega - P_o = C_p\left(\frac{1}{2}\,\rho_\alpha \upsilon_\omega^2\right) \tag{1}$$

where P_o is the reference pressure, C_p is the wind pressure coefficient, ρ_α is air density, and υ_ω^2 is wind velocity at the building height. Studies by Liddament [38] and CIBSE provide reference C_p values for low-rise buildings, illustrating variations in wind pressure across different surfaces. In dynamic insulation systems, these wind-induced pressures directly influence heat flow. For a square low-rise building exposed to 5.7 m/s wind at an 8 m ridge height, with indoor pressure set to –10 Pa, the pressure difference across side walls becomes zero, resulting in contra-flux operation and very low effective U-values (0.0008 W/m²K on the windward side and 0.1 W/m²K on the leeward side). When wind speeds exceed 5.7 m/s, portions of the wall shift into pro-flux, increasing U-values significantly—up to 0.36 W/m²K at 9.0 m/s, higher than a well-sealed envelope (U = 0.2 W/m²K) [38]. If these external pressures penetrate the envelope, they may disrupt indoor pressure fields, reduce the performance of passive or active thermal systems, and increase infiltration, especially in buildings with ventilated cavities [5]. To address these variables, this research includes a full-scale test bed or mock-up box to isolate conditions such as solar radiation, wind, and rainfall. Controlled airflow enables accurate determination of the active R-value for use in energy simulations [56] [57]. Additionally, integrating site-specific wind speed distributions (e.g., Rayleigh curves) helps estimate how frequently the wall operates in high-loss pro-flux conditions [3]. Locating dynamic insulation in ceilings—where pressure fields are more stable—is another strategy for mitigating wind-related fluctuations.

Vol. 6, No. 2, pp. 170-193
Submit: 04-07-2025 |
Accepted: 29-12-2025 |
Publish: 31-12-2025 |

Despite growing interest in leveraging building mass and ventilated cavities, most research prioritizes floor and slab systems, while wall-based adaptations remain underdeveloped. Ventilated hollow-core slabs have well-documented thermal mass benefits, but equivalent wall systems lack validated studies and field evidence [1]. Reviews of dynamic insulation show three persistent knowledge gaps: reliance on simplified analytical models, lack of standardized metrics for active R-value measurement, and limited quantification of wind-induced transitions between contra-flux and pro-flux modes [34] [38]. These gaps pose risks for designers, as predictions of heat removal, airflow-dependent R-values, and annual energy performance remain uncertain—particularly in tropical climates, where external forcing differs from that in temperate climates [37]. This study addresses these issues through three main contributions: (1) an experimentally validated dataset and test protocol for active ventilated wall panels, including full-scale or hot-box testing with clear boundary conditions and uncertainty analysis; (2) a combined CFD and transient heat-transfer study to evaluate effects of cavity geometry, airflow, inlet temperature, and wind speed on effective thermal resistance; and (3) a practical design framework defining Rtotal(V) relationships, criteria for beneficial versus detrimental ventilation regimes, and site-specific recommendations for tropical savanna climates. Together, these contributions reduce uncertainty, provide validated design tools, and establish a reproducible methodology for future research and standardization.

Static insulation, although widely used, presents several limitations that reduce its long-term thermal performance [25]. Air leakage is a primary issue; insulation can settle or compress over time, creating voids that allow air infiltration, especially when installation is poorly executed [35]. Thermal bridging further undermines envelope performance by allowing conductive structural components to bypass insulation and accelerate heat transfer, thereby increasing energy loads [32]. Static systems also lack dynamic heat management, resulting in temperature stagnation, overheating in hot seasons, and overcooling in cold seasons, which increases HVAC demand and reduces comfort [27]. Dynamic insulation enables the building envelope to modulate its thermal transmittance in response to environmental conditions [18].

Acting as an integrated heat-exchange system rather than a passive barrier, dynamic insulation reduces HVAC loads, mitigates air leakage, and limits thermal bridging by redistributing heat flow. Its ability to regulate heat transfer directly addresses issues associated with static insulation, including overheating and overcooling. Numerous strategies incorporate air layers into envelopes to reduce conductive and radiative heat transfer [62]. Systems such as Trombe walls, double-skin façades, photovoltaic façades, multi-layer windows, and airflow windows have demonstrated significant reductions in surface temperatures and attenuation of heat flux. For example, Trombe wall studies show that occlusion devices can lower exterior temperatures by more than 30°C, while closing ventilation openings delays heat transfer. Porous exhaust-air insulation walls effectively reduce inward heat flux [57], and double-skin façades have been shown to reduce indoor temperatures [12].

Low-emissivity coatings in double glazing further diminish radiative heat transfer within air cavities [23]. Energy-saving building envelope strategies are commonly categorized according to whether the air layer is ventilated. Without ventilation, the stagnant air increases wall thermal resistance due to air's low conductivity [24]. With ventilation, unsteady convective heat transfer removes heat before it enters indoor spaces, significantly reducing heat flux—an effect amplified by higher airflow velocities [39]. Recent emphasis on energy efficiency and indoor comfort has renewed interest in passive and low-energy systems that minimize reliance on mechanical conditioning [6]. Increasing the effective thermal mass of building materials is a key strategy [60]. Systems such as the Ventilated Hollow Core Slab (VHCS), Active Hollow Core Slab (AHCS), or TermoDeck employ slab mass for thermal storage, enabling passive heating and cooling and maintaining indoor temperatures with minimal mechanical input [22].

Ventilated wall concepts further extend these principles. Hollow block ventilated walls [29] combine airflow with concrete hollow blocks to dissipate stored heat in summer and recover heat in winter. Their performance depends on airflow velocity, inlet temperature, and cavity size. Experimental validation shows that ventilated walls achieve inner surface temperatures of 24.8–27.0°C, reduce heat flux by more than 55%, and exhibit decrement factors as low as 0.209 at airflow

JICE Journal Innovation of Civil Engineering
Vol. 6, No. 2, pp. 170-193
Submit: 04-07-2025 |
Accepted: 29-12-2025 |
Publish: 31-12-2025 |

rates of 0.3 m/s. Larger cavities and moderate airflow velocities optimize performance, while inlet temperatures of 26°C remove up to 67.75% of heat. Recommended airflow velocities range from 1.8 m/s for natural cooling to 0.3 m/s for AC exhaust. The Interlocking Passive Brick Set [65] introduces a dynamically regulated passive cooling system featuring interconnected cavities that promote natural convection. Its U-values range from 0.0354 to 0.2246 W/m²·K, reflecting high insulation performance combined with effective heat dissipation.

Airflow rates of 0.0061–0.0179 CFM enable passive cooling, reducing reliance on HVAC systems and supporting adaptable configurations for varied climates. Ventilated building envelopes, whether passive or active, present a promising approach to enhancing thermal performance and energy efficiency [31]. Passive systems such as hollow-core walls and interlocking bricks already demonstrate the capability of ventilation cavities to manage heat transfer. However, most existing research focuses on passive ventilation driven by environmental conditions, which can limit performance in climates with low temperature differentials or unreliable airflow. A significant research gap remains in integrating active ventilation mechanisms directly into wall structures. Currently, mechanical ventilation exists at the building systems level (e.g., HVAC), rather than within individual envelope components. Embedding active airflow pathways within walls could reduce thermal lag, enable targeted heat removal, and improve performance in high-mass or extreme-climate buildings [46]. Such systems could also be paired with renewable energy sources (e.g., solar-powered fans) to operate with minimal energy input.

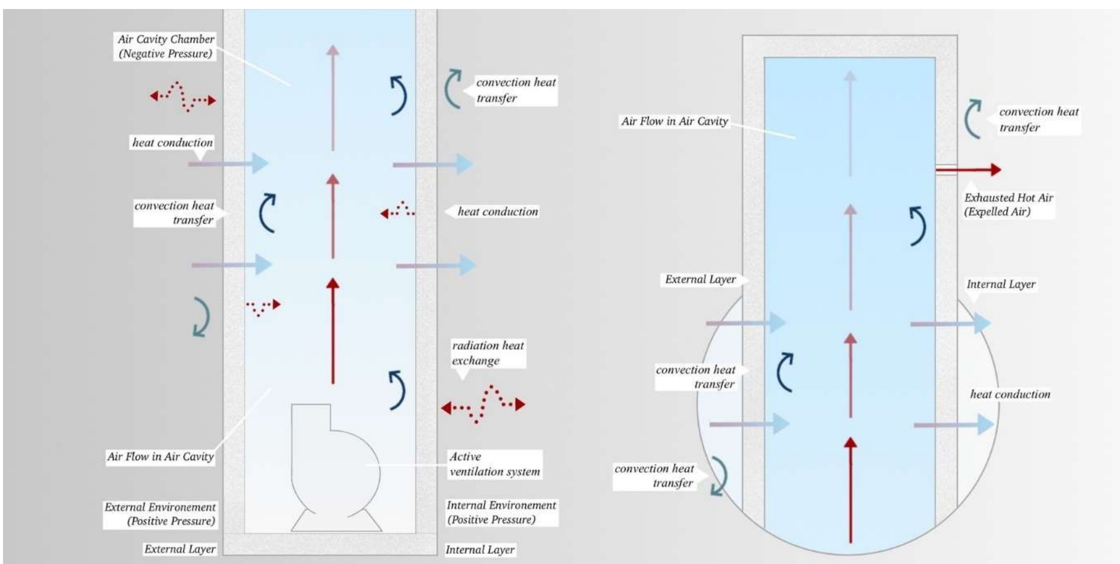

Figure 1. The schematic of the heat transfer, heat removal, and heat expulsion processes of the hollow precast wall on the right side of the diagram illustrates the schlieren imaging of thermal movement in the lower part of the building envelope, and the left side illustrates the thermal movement of the upper part.

2. Material and Method

The methodology for researching the hollow precast wall with active ventilation integrates theoretical modelling, CFD-based simulation, and a numerical experimental framework that functions as a substitute for physical testing. The system employs an air blower at the base of the wall that supplies cool air into the hollow core, forcing it upward through internal chambers where it absorbs heat before being expelled at the top. This forced convection dynamically reduces heat retention and enhances thermal mass behavior, offering significant advantages in hot climates where reducing HVAC dependence is essential [2][40]. The study is grounded in a quantitative modelling framework that couples predictive physics-based calculations with numerical simulation to align

JICE Journal Innovation of Civil Engineering
Vol. 6, No. 2, pp. 170-193
Submit: 04-07-2025 |
Accepted: 29-12-2025 |
Publish: 31-12-2025 |

theoretical predictions with experimental analogs and to refine key parameters governing heat transfer and airflow [55][49]. Initial analysis focuses on material characterization—thermal conductivity, density, specific heat, and diffusivity of lightweight concrete and air—which enables application of Fourier's Law and the transient heat diffusion equation to evaluate temperature gradients and unsteady heat conduction. Empirical boundary and initial conditions are incorporated to calibrate and validate theoretical outputs [44][15].

A three-track integrated methodology is adopted: (a) analytical and transient heat-transfer modelling to establish baseline behavior, dimensionless parameters, and conduction–convection interactions; (b) high-resolution CFD and conjugate heat-transfer (CHT) simulation to resolve coupled air–solid dynamics within the cavity and across wall surfaces; and (c) numerical "virtual" experimentation to generate validation data and quantify uncertainty. The analysis includes detailed 3D geometry definition, material property specification, and buoyancy modeling using either the Boussinesq approximation or full temperature-dependent density.

CFD simulations are conducted using validated solvers (ANSYS Fluent, COMSOL, or OpenFOAM) with pressure-based transient algorithms, RANS (k–ω SST) for parametric studies, and LES for selected high-fidelity cases. Radiative exchange is captured through view-factor or DO radiation models, and the solver resolves full conjugate heat transfer across concrete layers and the cavity air. Mesh independence, time-step independence, and Richardson extrapolation ensure numerical accuracy. Boundary conditions replicate realistic indoor and outdoor environments, including ambient temperature variation, wind-induced pressure, and prescribed inlet temperatures or mass flow rates.

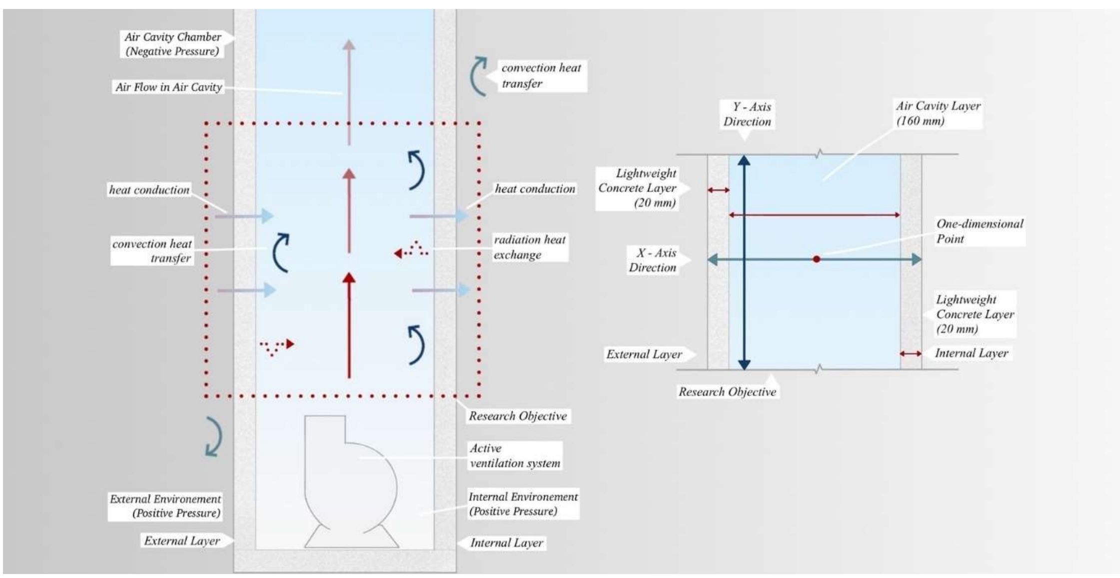

Figure 2. Schematic of the Research Objectives for the hollow precast wall: The right side of the diagram illustrates the research objectives across three dimensions: the x-axis, the y-axis, and a one-dimensional point. The left side represents the broader scope of the research objective, focusing on thermal movement.

Dimensionless analysis employs Fourier and Biot numbers to characterize transient conduction and the conduction–convection interface. Radiative exchange applies Kirchhoff's Law and the Stefan-Boltzmann Law, while convective heat transfer uses Nusselt number correlations based on Reynolds and Prandtl numbers. Stack-effect-driven mass flow and Reynolds number calculations classify the airflow regime and quantify the blower's contribution to thermal performance. Wind-speed-dependent thermal resistance is evaluated by relating forced-convection enhancement to changes in convective heat transfer coefficients. Baseline thermal resistance is calculated under still

Vol. 6, No. 2, pp. 170-193
Submit: 04-07-2025 |
Accepted: 29-12-2025 |
Publish: 31-12-2025 |

air; increments in wind velocity modify internal and external convective coefficients according to empirical power-law functions [63] [10]. Results show sharp reductions in R-value during the transition from natural to forced convection, followed by gradual stabilization as wind speed increases, characterizing the dynamic response of the active envelope [14]. Verification and validation rely on benchmarking against analytical solutions and published experiments on ventilated walls and cavity flows [29] [39] [45].

A numerical "virtual hot-box" estimates active R_total(V) by imposing tightly controlled interior–exterior boundary conditions and converting simulated heat fluxes to equivalent R-values, ensuring methodological comparability with standardized hot-box testing. Uncertainty quantification uses Monte Carlo or Latin Hypercube sampling on thermal properties, emissivity, inlet temperature, and flow rate; sensitivity analysis identifies the dominant parameters influencing R_total(V) and surface-temperature performance. Outputs include temperature fields, heat-flux distributions, cavity mass-flow rates, radiation contributions, Nusselt numbers, and R_total(V) curves for varying ventilation rates and wind speeds. These results establish operating envelopes, highlight regimes where ventilation is beneficial or potentially counterproductive, and compare performance against literature benchmarks. Limitations related to the absence of new physical experiments, long-term material behavior, and complex multi-building aerodynamics are acknowledged. Future work is directed toward integrating mechanical ventilation components into wall systems while maintaining structural, energy, and economic feasibility [28].

A hollow precast wall is a building material used to construct walls, the building envelope, and other elements in prefabricated construction. The dimension of an active double-layered precast wall is 240 x 20 x 100 cm. The wall model is tabulated below (Fig. 1).

Table 1. Physical parameters of the wall material

Layer	Height (cm)	Length (cm)	Thickness (cm)	Density (kg/m^3)	Specific heat (J/kg*K)	Thermal Conductivity (W/mK)
Air Cavity	240.00	96.00	16.00	600	1000	0.19
Lightweight Concrete	240.00	100.00	20.00	1.293	1005	0.02596

2.1. The design of the hollow precast wall

The hollow precast wall panel is designed with an integrated air blower strategically positioned at the base of the air-cavity channel. This system facilitates airflow through the cavity, effectively expelling accumulated heat through an exhaust outlet at the top and functioning as a dynamic insulation mechanism. The panel features a central air gap within its structure, enhancing both its thermal performance.

2.2. The principle of the hollow precast wall

The hollow precast wall incorporates interconnected air cavities, active ventilation channels, and airflow pathways to enhance heat removal from the building envelope [47]. Warm air rises through internal channels and exits at the top, while cooler air descends, creating a self-regulating airflow that acts as dynamic insulation. This mechanism balances heat transfer by enabling controlled circulation within the wall system. Heat transfer occurs through conduction, convection, external heat exchange, and enthalpy flow within the ventilated cavity. Conduction occurs across the internal and external layers, while the cavity facilitates heat transfer between the facing surfaces. For analytical simplification, three assumptions are applied:

1. Vertical heat conduction (y-direction) is negligible, with conduction occurring primarily along the x-direction.
2. Airflow in the cavity is treated as two-dimensional, with humidity effects ignored due to warm air expulsion.

JICE Journal Innovation of Civil Engineering
Vol. 6, No. 2, pp. 170-193
Submit: 04-07-2025 |
Accepted: 29-12-2025 |
Publish: 31-12-2025 |

3. All solid materials are considered homogeneous, isotropic, and with constant thermal properties.

2.3. Experiment: theoretical calculation of thermal properties of hollow precast wall

Before the hollow precast wall can function as intended, it must first absorb heat at the exposed surface. This initial heat-uptake stage is often overlooked in dynamic-insulation theory, yet the experiment in this section shows its importance for both thermal performance and structural behavior. The air cavity is 160 mm wide and 2400 mm high, with a 10 mm exhaust opening at the top and a matching 10 mm blower inlet at the bottom. This geometry promotes efficient upward airflow, improving heat removal and enhancing the wall's overall energy performance.

2.4. Research objectives

The research objective is to examine heat transfer and airflow within the hollow precast wall across three dimensions: the x-axis, the y-axis, and a one-dimensional point representing key dimensionless parameters. Along the x-axis, the study evaluates conductive, radiative, and resistive heat transfer through the building envelope [20], including heat flux across layers, radiative exchange based on Kirchhoff's Law and the Stefan-Boltzmann Law, and the overall heat transfer coefficient to assess insulation performance [52]. Along the y-axis, the analysis focuses on vertical airflow driven by the stack effect. Airflow rates, temperature gradients, and pressure differences inside the cavity are examined to characterize buoyancy-induced ventilation, supported by CFD simulations and experimental results to optimize passive cooling. The one-dimensional point considers key dimensionless numbers—primarily the Nusselt and Prandtl numbers—which represent convective heat-transfer efficiency and airflow behavior in the cavity [36]. Together, these three analytical dimensions provide an integrated framework for improving the wall panel's thermal efficiency and enhancing passive cooling in sustainable building design.

2.5. Numerical model for theoretical thermal calculation

For steady-state in one-dimensional conduction

$$q = -k\frac{\triangle T}{\triangle x} \tag{2}$$

Where q is heat flux [W/m²], $\partial T/\partial x$ is temperature gradient [K/m], k is thermal conductivity [W/m·K]. Divide the wall into segments: Light weight concrete (layer 1 with thickness of 0.02 m), air cavity (layer 2 with thickness of 0.16 m), and Light weight concrete (layer 3 with thickness of 0.02 m).

$$R_{th,layer} = \frac{\triangle x}{k} \tag{3}$$

Where R is thermal resistance [K/W], k is thermal conductivity [W/m·K], $\triangle x$ is the thickness of the layer, [m]. With a total thermal resistance which is $R_{concrete} + R_{air} + R_{concrete}$ to further find the heat flux with a temperature difference of 2°C between the two sides of the wall. If the temperatures on the two opposite sides are 313.15 K (outside the building) and 293.15 K (inside the building).

$$q = \frac{\triangle T}{R_{total}} \tag{4}$$

Where $q$is heat flux [W/m²], $\Delta T$is the temperature difference [K], and $R_{total}$is the total thermal resistance [K/W]. To determine the temperatures at the four points (outside of concrete layer 1, inside of concrete layer 1, inside of concrete layer 2, and outside of concrete layer 2), steady-state heat transfer is applied using the thermal resistances of each layer. The boundary conditions are: outside surface temperature $T_{out} = 313.15$ K, inside surface temperature $T_{in} = 293.15$ K, and convective

Vol. 6, No. 2, pp. 170-193
Submit: 04-07-2025 |
Accepted: 29-12-2025 |
Publish: 31-12-2025 |

coefficients $h_{\text{out}}$and h_{in}[W/m²·K]. Both convective and conductive resistances are used to compute the temperature at each interface.

a) Convective Resistance

$$R_{conv,out} = \frac{1}{h_{outside}} \qquad R_{conv,in} = \frac{1}{h_{inside}} \tag{5}$$

b) Conductive Resistance

$$R_{cond,concrete} = \frac{L_{concrete}}{k_{concrete}} \qquad R_{cond,air} = \frac{L_{air}}{k_{air}} \tag{6}$$

c) Total Thermal Resistance

$$R_{total} = R_{conv,out} + R_{cond,concrete} + R_{cond,air} + R_{cond,concrete} + R_{conv,in} \tag{7}$$

Where $L_{concrete}$ is the length of the concrete layer [m], L_{air} is the length of the air cavity layer [m], $K_{concrete}$ is the thermal conductivity of the concrete layer [W/m·K], K_{air} is the thermal conductivity of the air cavity layer [W/m·K]. As Convective heat transfer coefficients assigned as the following; h_{out} is 10 W/m²·K and h_{in} is 25 W/m²·K according to the average point of the natural ventilation and low point on forced ventilation. Connective Resistance for the outside layer $R_{conv,out} = 0.1\, m^2 \cdot$ K/W, for the inside layer $R_{conv,in} = 0.04\, m^2 \cdot$ K/W. Conductive resistance for each concrete layer $R_{cond,concrete} \approx 0.77\, m^2 \cdot$ K/W, and for the air cavity $R_{cond,concrete} \approx 0.77\ m^2 \cdot$ K/W. therefore, $R_{total} = 1.696\, m^2 \cdot$ K/W. With the provided information, the heat flux through the wall is constant in steady-state conditions use the following equation:

$$q = \frac{T_{outside} - T_{inside}}{R_{total}} \tag{8}$$

Where q is heat flux [W/m²], $T_{outside}$ is the temperature outside the building envelope [K], T_{inside} is temperature inside the building envelope [K], R_{total} is total thermal resistance [K/W]. With provided information with defined value $q \approx 11.80\, \mathrm{W/m^2}$. Using the heat flux q, calculate the temperature drops across each resistance for the temperature at each point:

1) Temperature Drop Across Outside Convective Resistance:

$$T_1 = T_{outside} - q \cdot R_{conv,out} \tag{9}$$

2) Temperature Drop Across Concrete Layer 1:

$$T_2 = T_1 - q \cdot R_{cond,concrete} \tag{10}$$

3) Temperature Drop Across Air Cavity:

$$T_3 = T_2 - q \cdot R_{cond,air} \tag{11}$$

4) Temperature Drop Across Concrete Layer 2:

$$T_4 = T_3 - q \cdot R_{cond,concrete} \tag{12}$$

Vol. x, No. x, pp. xx-xx, xxxx
Submit: xx-xx-xxxx |
Accepted: xx-xx-xxxx |
Publish: xx-xx-xxxx |

5) Temperature Drop Across Inside Convective Resistance:

$$T_{inside} = T_4 - q \cdot R_{conv,in} \tag{13}$$

Figure 3. Illustration of the point of temperature at each location within building envelope; ranging from external (T1) and internal layers (T4).

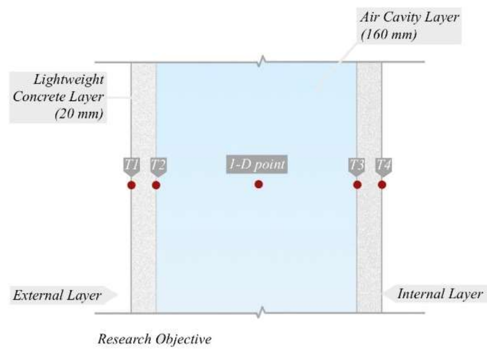

Table 2. The point of temperature at each location within building envelope

Pts	T1 (K)	T2 (K)	T3 (K)	T4 (K)
Temps	311.97	302.88	293.80	284.24

Where T_{th} is the point of temperature at each location within the building envelope [K], q is heat flux [W/m²]. With the provided information, the point of temperature is shown as $T_1 = 311.97\ K, T_2 = 302.88\ K, T_3 = 293.80\ K$, and $T_4 = 284.24\ K$. To further comprehend Unsteady Heat Conduction with the interval of time. At the starting time = 0 s, the temperature of the concrete surface is 312.843K; after time = 1800 s, the temperature of concrete surface is 318.706K**;** after time = 3600 s, the temperature of the concrete surface is 324.817K. With three-time interval to consider create rate of temperature change with time with following equation;

$$\frac{\partial T}{\partial t} \approx \frac{T_2 - T_1}{t_2 - t_1} \tag{14}$$

Where $\partial T/\partial t$is the temperature-change rate [K/s], $T_1, T_2$are temperatures at times t_1, t_2[s]. For interval 1 ($t_1 = 0$, $t_2 = 1800$), $\partial T/\partial t \approx 0.00326$ K/s. For interval 2 ($t_1 = 1800$, $t_2 = 3600$), $\partial T/\partial t \approx 0.00340$ K/s. The average rate over the full 3600 s, using temperatures at $t = 0$and $t = 3600$, is $\partial T/\partial t \approx 0.00333$ K/s.To compute the second spatial derivative of temperature within the concrete, the finite-difference approximation is applied as follows:

$$\frac{\partial^2 T}{\partial x^2} \approx \frac{T_{i-1} - 2T_i + T_{i+1}}{\triangle x^2} \tag{15}$$

Where $\partial^2 T/\partial x^2$ is second derivative of temperature with respect to position [K/ m²], T_{i-1} is Temperature at the previous spatial point [K], T_i is Temperature at the current point [K], T_{i+1} is Temperature at the next spatial point [K], $\triangle x$ is Distance between points [m]. With temperature values at three or more points along the x-axis. As $T_{i+1} = 312.843K$, $T_i = 318.706K$, $T_{i+1} = 324.817K$ with distance of the building envelope is 0.2 m. Finalize the $\partial^2 T/\partial x^2 \approx 6.2$ K/ m^2 . Set overall thermal conductivity as 0.0323 W/m·K from $k_{total} = L_{total}/R_{total}$, and find thermal diffusivity using the following equation;

Vol. x, No. x, pp. xx-xx, xxxx
Submit: xx-xx-xxxx |
Accepted: xx-xx-xxxx |
Publish: xx-xx-xxxx |

$$\alpha \frac{k}{\rho C_p} \tag{16}$$

Where α is thermal diffusivity [m^2/s], ρ is density [kg/m^3], C_p is specific heat capacity [j/kg·K]. Set overall thermal conductivity as 0.0323 W/m·K. To find overall density, specific heat, use the following equation (in one dimensional model):

$$\rho_{total} = \frac{\sum(\rho_i \cdot L_i)}{\sum L_i} \tag{17}$$

$$C_{p_{total}} = \frac{\sum(C_{p_i} \cdot \rho_i \cdot L_i)}{\sum \rho_{total} \cdot L_i} \tag{18}$$

Where the building envelope consists of: Lightweight concrete (2 layers, 0.02 m each), Air cavity (0.16 m), L_i is the thickness layer of material. The result ρ_{total} is approximately 280.98 kg/m^3 and $C_{p_{total}}$ is approximately 2095.7 j/kg·K. With provided information, thermal diffusivity of the building envelope equal $5.48 \times 10^{-8}\, m^s/s$. With all the provided information, Equation for Unsteady Heat Conduction can be use.

$$\frac{\partial T}{\partial t} = \alpha \frac{\partial^2 T}{\partial x^2} \tag{19}$$

Where $\partial T/\partial t$ is Rate of temperature change with time [K/s], α is thermal diffusivity [m^2/s], $\partial^2 T/\partial x^2$ is second derivative of temperature with respect to position [K/ m²].

$$\rho C_p \frac{\partial T}{\partial t} = k \frac{\partial^2 T}{\partial x^2} \tag{20}$$

Where ρ is density [kg/m^3], C_p is specific heat capacity [j/kg·K], $\partial T/\partial t$ is Rate of temperature change with time [K/s], k is thermal conductivity [W/m·K], $\partial^2 T/\partial x^2$ is second derivative of temperature with respect to position [K/ m²]. Set overall thermal conductivity as 0.0323 W/m·K from $k_{total} = L_{total}/R_{total}$ and $\partial^2 T/\partial x^2 \approx 6.2$ K/ m^2. thermal diffusivity of the building envelope equal $5.48 \times 10^{-8}\, m/s$. The result of the rate of temperature change with respect to time is approximate 3.40×10^{-7} K/s. With the information provided, the context is enough to be able to find dimensionless number which are The Fourier number is a dimensionless number that represents the ratio of heat conduction to heat storage in a material given by:

$$F_o = \frac{\alpha t}{L^2} \tag{21}$$

Where F_o is Fourier number, α is thermal diffusivity of the material [m^2], t is time [s] (time period of 3600 seconds), and L is characteristic length (thickness of the building envelope) [m]. Fourier number is approximate 4.932\times{10}^{-3}. Another dimensionless number is Biot Number that represents the ratio of conduction resistance within a solid to convective resistance at its surface given by:

$$B_i = \frac{hL}{k} \tag{22}$$

JICE Journal Innovation of Civil Engineering
Vol. 6, No. 2, pp. 170-193
Submit: 04-07-2025 |
Accepted: 29-12-2025 |
Publish: 31-12-2025 |

Where Bi is Biot number, h is Convective heat transfer coefficient [W/m^2·K], L is characteristic length (thickness of the building envelope) [m], k is thermal conductivity [W/m·K]. Biot number is approximate ≈ 61.91. To calculate, solve Kirchhoff's Law of Radiation state, it requires solving heat transfer by radiation between the two interval points. Interval 1: Between the exterior (outside concrete layer) and the air cavity. Interval 2: Between the air cavity and the interior (another outer layer of concrete), the Stefan-Boltzmann law is used:

$$q_{rad} = \sigma \cdot F_{12} \cdot A \cdot (T_1^4 - T_2^4) \tag{23}$$

Where q_{rad} is heat transfer by radiation [W], σ is Stefan-Boltzmann constant equal $5.67 \times 10^{-8}\, W/m^2 \cdot K^4$, A is surface area (m^2), T_{th} is the surface temperatures in Kelvin. The interval 1 is $T_1 = 312.834\, K$, $T_2 = 312.787\, K$, and interval 2 is $T_3 = 293.242\, K$, and $T_4 = 293.195\, K$. Assume F_{12} = 1 for full view exchange. The heat transfer by radiation of interval 1 equal 0.408 W and interval 2 equal 0.272W. To apply Kirchhoff's Law of Radiation, it is necessary to determine emissivity and absorptivity.

$$\varepsilon(\lambda, T) = \alpha(\lambda, T) \tag{24}$$

Where $\varepsilon(\lambda, T)$is spectral emissivity, $\alpha(\lambda, T)$is spectral absorptivity, $\lambda$is wavelength [m], and $T$is absolute temperature [K]. For concrete, $\varepsilon = 0.85$and $\alpha = 0.85$ (per Kirchhoff's law). With emissivity known, the net radiative heat transfer is given by:

$$q_{rad} = \varepsilon \cdot \sigma \cdot F_{12} \cdot A \cdot (T_1^4 - T_2^4) \tag{25}$$

Where q_{rad} is heat transfer by radiation [W], σ is Stefan-Boltzmann constant equal $5.67 \times 10^{-8}\, W/m^2 \cdot K^4$, A is surface area (m^2), T_{th} is the surface temperatures in Kelvin. The interval 1 is $T_1 = 312.834\, K$, $T_2 = 312.787\, K$, and interval 2 is $T_3 = 293.242\, K$, and $T_4 = 293.195\, K$. Assume F_{12} = 1 for full view exchange. The heat transfer by radiation of interval 1 equal 0.347 W and interval 2 equal 0.231 W.

Since the core of this dynamic building envelope is the integration of active ventilation system embedded at the base of the building envelope's air cavity. Assume that there is an air blower that produce 0.1 m/s (an average speed of small air blower) with opening of 0.1 m^2. For the relative humidity, it is 73%, which is an average for a hot-humid climate region. The mass flow rate equation is given as:

$$\dot{m} = \rho \cdot V \cdot A \tag{26}$$

Where ṁ is mass flow rate [kg/s], ρ is air density [kg/m^3], V is air velocity [m/s], and A is opening area [m^2]. With provided information mass flow rate is equal 0.0126 kg/s. To predict fluid flow patterns in different situations by measuring the ratio between inertial and viscous forces, incorporate Reynolds number given as:

$$\text{Re} = \frac{\rho \cdot V \cdot D_h}{\mu} \tag{27}$$

Where Re is Reynolds Number, ρ is air density [kg/m^3], V is air velocity [m/s], D_h is characteristic of linear dimension of Hydraulic diameter, μ is dynamic viscosity of air at room temperature [$1.85 \times 10^{-5} Pa \cdot s$]. First step is finding D_h using the following:

$$D_h = \frac{4A}{P} \tag{28}$$

JICE Journal Innovation of Civil Engineering
Vol. 6, No. 2, pp. 170-193
Submit: 04-07-2025 |
Accepted: 29-12-2025 |
Publish: 31-12-2025 |

Where D_h is characteristic of linear dimension of Hydraulic diameter [m], A is opening area [m], P is Wetted perimeter (depends on geometry). Assuming the opening is a square for simplicity where side length L = $\sqrt{A}$ = $\sqrt{0.1} \approx 0.316\, m^2$ with wetted perimeter equal 1.264 m^2. Where characteristic of linear dimension of Hydraulic diameter is 0.316 m. As a result, the Reynolds number is approximately 2,091. Given the building envelope with an air cavity, the stack effect would be applied to its design. Pressure difference due to the stack effect:

$$\triangle \mathrm{P} = \rho \cdot g \cdot ht \cdot \frac{T_i - T_o}{T_i} \tag{29}$$

Where $\triangle$ P is Pressure difference [Pa], ρ is Air density [kg/m³], g is Acceleration due to gravity [9.81m/s^2], h is height of the column of air [m], T_i is inside temperature [K], T_o is outside temperature [K]. As the Height of the building envelope (h): 2.4 m, with inside temperature of 293.242 K, and outside temperature of 312.834 K. Air density is 1.225 kg/m^3, Cross-sectional area of the opening is 0.18 m, Discharge coefficient is 0.6. The result of Pressure difference is $\triangle$ P $\approx$ $0.97\ Pa$

$$\mathrm{Q} = C_d \cdot A \cdot \sqrt{\frac{2 \triangle \mathrm{P}}{\rho}} \tag{30}$$

Where Q is volumetric airflow rate [m³/s], C_d is discharge coefficient (typically ~0.6–0.65 for most openings), A is Cross-sectional area of the opening [m²], △P is pressure difference [Pa], ρ is air density [kg/m³]. In this case Discharge coefficient is 0.65 (typical for openings), Opening area is 0.1 m2, Pressure difference is 0.979 Pa from the previous equation. The approximate Volumetric Flow Rate is 0.0823 m3/s. With this information the Prandtl number as the ratio of momentum diffusivity to thermal diffusivity

$$Pr = \frac{\mu \cdot C_p}{k} \tag{31}$$

Where Pr is Prandtl number, μ is the dynamic viscosity of air [Pa·s], C_p is the specific heat capacity of air [J/kg·K], k is the thermal conductivity of air [W/m·K]. Where C_p approximate is 1005 J/kg·K, k approximate is 0.026 W/m·K, μ is dynamic viscosity of air at room temperature $[1.85 \times 10^{-5} Pa \cdot s]$. The Prandtl number ($Pr$) for air is approximately 0.715. With the Prandtl number Nusselt number which the ratio of total heat transfer to conductive heat transfer at a boundary in a fluid could be given by the following empirical correlation:

$$Nu = 0.023 \cdot Re^{0.8} \cdot Pr^{0.4} \tag{32}$$

Where Nu is Nusselt number, Re is the Reynolds number, Pr is Prandtl number. The Reynolds number is approximately 2,091, and the Prandtl number for air is approximately 0.715. The Nusselt number (Nu) is approximately 9.114513. With the provided information the heat transfer coefficient (h) can be calculated from the Nusselt number (Nu) and the hydraulic diameter (Dh) be given by the equation:

$$h = \frac{Nu \cdot k}{D_h} \tag{33}$$

Where h is heat transfer coefficient [W/m^{2}K], Nu is the Nusselt number, k is the thermal conductivity of the fluid (air in this case) [W/m·K], Dh is the hydraulic diameter [m]. The Nusselt number (Nu) is approximately 9.114513, k approximate is 0.026 W/m·K, and $D_h \approx 0.316\, m$. The result of heat transfer coefficient approximate is 0.749928303 W/m^{2}K

Write a formula to find Thermal resistance over time and with wind speed. for a wall envelope with an integral time-heat transfer that gradually transfers, with wind pumping in at the bottom. To see how speed of wind pumping interacts with the heat transfer and thermal resistance

Vol. x, No. x, pp. xx-xx, xxxx
Submit: xx-xx-xxxx |
Accepted: xx-xx-xxxx |
Publish: xx-xx-xxxx |

$$R_{cond} = \frac{L}{k} \tag{34}$$

Where L is the wall thickness [m], and k is its thermal conductivity [W/m·K]. L determined as 0.2 m, and using total thermal conductivity as 0.0323 W/m·K the convective resistance, which is strongly influenced by wind speed, is defined as

$$R_{conv}(V) = \frac{L}{h(V)\,A} \tag{35}$$

with A representing the surface area available for convection [m^2], and the convective heat transfer coefficient h (V) [W/m^{2}K], modeled as a function of wind speed V [m/s]. A common empirical relationship for h(V) is.

$$\mathrm{h\,(V)} = h_0 + \alpha V^n \tag{36}$$

Here, $h_0$is the natural-convection baseline coefficient, while $\alpha$and $n$are empirical constants describing wind-driven enhancement. The exponent $n$indicates the sensitivity of the convective coefficient to wind speed, typically ranging from 0.5–0.8 for turbulent forced convection on building surfaces, with 0.6 commonly used for moderately turbulent outdoor conditions. The coefficient αreflects the magnitude of wind-induced enhancement and depends on surface geometry, roughness, and environmental conditions; a representative value is $\alpha = 0.5$.

In this study, $h_0 = 2$ W/m^2K, $n = 0.6$, and $\alpha = 0.5$, yielding a convective heat transfer coefficient of 2.125594 W/m^2K. The corresponding steady-state thermal resistance is then:

$$R_{total}(V) = \frac{L}{k} + \frac{1}{A\,(h_0+\alpha V^n)} \tag{37}$$

Where $R_{total}(V)$ is Total thermal resistance [W/K]. When considering the transient response of the wall envelope, the energy balance for a lumped system is written as

$$C\frac{dT}{dT} = \frac{T_\infty - T(t)}{R_{total}\,(V)} \tag{38}$$

Where C is the thermal capacitance of the wall [J/K], T(t) is its temperature at time t [K [s]], and $T\infty$ is the ambient temperature [K]. Solving this first-order differential equation yields. Where T_∞ is 313.15 K according to the surface on one side, and $T(t)$ is 307.390 K from the following equation and R total as 3.781 W/K. Which thermal capacitance is equivalent to 0.6594 J/K.

To find Ambient temperature conditions, using convective heat transfer equation. For

$$q_{conv} = hA\,(T_s - T_{amp}) \tag{39}$$

Where q_{conv} is convective heat transfer [W/m^{2}K], h is Heat transfer coefficient [W/m^{2}K], A is Area exposed to air [m^2] T_s is Surface temperature [K], T_{amp} is Ambient temperature [K], Rearrange to;

$$T_{amp} = T_s - (\frac{q_{conv}}{hA}) \tag{40}$$

Journal Innovation of Civil Engineering
Vol. 6, No. 2, pp. 170-193
Submit: 04-07-2025 |
Accepted: 29-12-2025 |
Publish: 31-12-2025 |

Where T_{amp} is ambient temperature [K] (this variable will be used in the part of temperature at that time in the other equation. As the convective coefficient under natural convection is 25 W at wind speed outside of 1 m/s, n as 0.6 and α equal of 0.5. As a result, the convective heat transfer coefficient is 5.5 W/m²K. With surface temperature of 313.5 K, the ambient temperature (temperature at that time) equal to 311.2561 K.

$$\mathrm{T(t)} = T_\infty + (T(0) - T_\infty)\, exp(-\frac{t}{T}) \tag{41}$$

In this equation, $T(t)$ is the temperature of the system at time t. The term $T\infty$ represents the steady-state temperature that the system will eventually reach when it has fully equilibrated with its surroundings. The value $T(0)$ is the initial temperature of the system at time t = 0. The exponential term, $exp(-\frac{t}{T})$, describes the decay of the temperature difference between the system and its surroundings over time. Here, τ is the time constant, a key parameter that determines how fast the temperature approaches $T\infty$. As EXP(x) returns the natural exponential of x. where e is the base of the natural logarithm, 2.71828 (Euler's number). EXP is the inverse function of the LN function. Steady-state temperature equal to 310.881 K with initial temperature at 313.15 K. t is equal to 1800s and T as 3600s. Temperature at time constant equal 312.4048 K.
with the time constant τ defined as below.

$$\tau = R_{total}(V)C = \left[\frac{L}{k} + \frac{1}{A\,(h_0 + \alpha V^n)}\right]C \tag{42}$$

This formula shows that an increase in wind speed V increases the convective heat transfer coefficient $h(V)$, thereby reducing Rconv and, consequently,ly the overall thermal resistance Rtotal(V). As a result, the time constant τ decreases, meaning that the wall envelope will respond more quickly to changes in ambient conditions. In summary, the transient temperature behavior of the wall envelope, influenced by wind-induced convection, is given by

$$\mathrm{T(t)} = T_\infty + (T(0) - T_\infty)\, exp\left\{-\frac{t}{C\left[\frac{L}{k} + \frac{1}{A\,(h_0 + \alpha V^n)}\right]}\right\} \tag{43}$$

3. Result and Discussion

The material properties used in the analysis correspond to the x-axis section of the hollow precast wall, with supporting data provided in the tables, figures, and Section 5. The observed reduction in U-value under forced convection aligns with prior findings for ventilated wall systems. Earlier studies reported a 20–30% decrease in thermal transmittance at low cavity-air velocities, and the present 27.6% reduction at 0.1 m/s falls within this range. Yao et al. [61] similarly noted that the greatest gains occur during the transition from natural to forced convection, confirming that minimal airflow disrupts boundary-layer formation and validating the modeling approach.

The thermal-resistance and U-value curves (Figures 3 and 4) show strong nonlinearity at low velocities (0–0.5 m/s), reflecting transitional mixing. At higher velocities (2–10 m/s), improvements diminish, consistent with Brida et al. [10], who showed that once Reynolds numbers exceed ~2000, performance becomes limited by solid-phase conduction. Low-velocity airflow therefore provides the most efficient enhancement.

Vol. 6, No. 2, pp. 170-193
Submit: 04-07-2025 |
Accepted: 29-12-2025 |
Publish: 31-12-2025 |

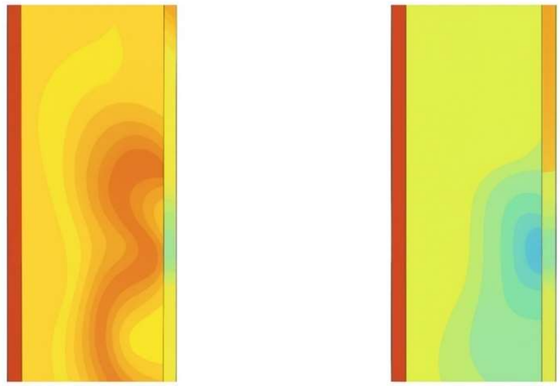

Figure 4. illustrates via computational simulation the thermal performance of the active double-layer wall panel under two airflow conditions: (a) zero wind speed and (b) a low wind speed of 0.1 m/s.

The wall's thermal conductivity (λ = 0.032 W/mK) is comparable to aerated autoclaved concrete (0.030–0.045 W/mK) [9], while the addition of active ventilation offers dynamic behavior not achievable with static insulation.

Table 3. Theoretical Calculation of the hollow precast wall numerical data of the variable that required for additional numerical input ranging from total density, total heat capacity, thermal conductivity, etc.

	ρ (kg/m^3)	Cρ (J/Kg·K)	λ (W/m·K)	R (K/W)	q (W/m^2)	Tin (K)	Tout (K)
A.1	3.049	2095.7	0.032	1.696	11.800	293.150	313.150

Uncertainties include uniform boundary-condition assumptions, ±15% wind-driven fluctuations [14], and ±10% variability in lightweight-concrete conductivity. Conservative error margins of ±0.02 W/m²K (U-value) and ±0.15 K/W (resistance) are therefore appropriate. One-dimensional modeling introduces additional limitations; Amar et al. [7] demonstrated that junctions can raise local U-values by up to 12%, indicating the need for prototype validation.

Wind dependency also introduces operational variability. In a Köppen Aw climate, calm periods may reduce performance to natural-convection levels (U = 0.590 W/m²K), while high winds may exceed modeled conditions. Longer-term climate-based simulations and potential integration of low-energy fans are recommended to ensure stable airflow and consistent performance.

3.1. Thermal Properties Analysis

The thermal properties assessment confirms that the hollow precast wall is well suited for energy-efficient construction in hot climates. Its very low density (3.049 kg/m³) and high air content contribute to strong insulation, supported by a low thermal conductivity of 0.032 W/m·K, comparable to lightweight insulating materials [9]. The resulting thermal resistance of 1.696 K/W and a heat flux of 11.8 W/m² under the indoor–outdoor gradient (293.15–313.15 K) indicate controlled heat transfer and effective thermal moderation.

Dimensionless parameters further validate this behavior. The Fourier number (Fo = 4.932 × 10^{-3}) indicates slow heat diffusion, while the Biot number (Bi = 61.9) confirms large internal gradients and conduction-dominated transfer, both contributing to delayed heat penetration. Airflow conditions yield a Reynolds number of 2091 (laminar), producing a low convective coefficient (h = 0.745 W/m²·K). The Nusselt number (Nu = 9.114) reflects modest convective enhancement, and the Prandtl number (Pr = 0.715) aligns with typical air behavior.

JICE Journal Innovation of Civil Engineering
Vol. 6, No. 2, pp. 170-193
Submit: 04-07-2025 |
Accepted: 29-12-2025 |
Publish: 31-12-2025 |

Table 4. Theoretical Calculation of the Interlocking Passive Brick Set numerical data of the variable that required for additional numerical input ranging from total density, total heat capacity, thermal conductivity, etc

	Fo	Bi	m (kg/s)	Re	Pr	Nu	h (W/m^2 K)
A.1	4.932*10^-3	61.9	0.013	2091	0.715	9.114	0.745

The wall's combination of low conductivity, high resistance, slow diffusion, and limited convection makes it a strong passive-insulation option. These characteristics support reduced cooling loads and improved indoor comfort relative to many conventional insulating systems.

3.2. Component Performance Analysis

The study evaluates the thermal resistance behavior of the wall envelope over time under varying wind speeds, focusing on how forced convection from the bottom interacts with internal conduction and convection. Thermal resistance is a key measure of insulation effectiveness [54], combining both conductive resistance through the solid and convective resistance at the surface.

Table 5. The point of difference thermal resistance at each wind speed within building envelope

Wind speed (m/s)	Rtotal (K/W)
0.0	1.696
0.1	3.781
0.5	3.985
1.0	4.155
1.5	4.293
2.0	4.413
2.5	4.521
3.0	4.622
3.5	4.715
4.0	4.804
4.5	4.888
5.0	4.968
5.5	5.046
6.0	5.120
6.5	5.192
7.0	5.262
7.5	5.330
8.0	5.396
8.5	5.461
9.0	5.524
9.5	5.585
10.0	5.646

Vol. 6, No. 2, pp. 170-193
Submit: 04-07-2025 |
Accepted: 29-12-2025 |
Publish: 31-12-2025 |

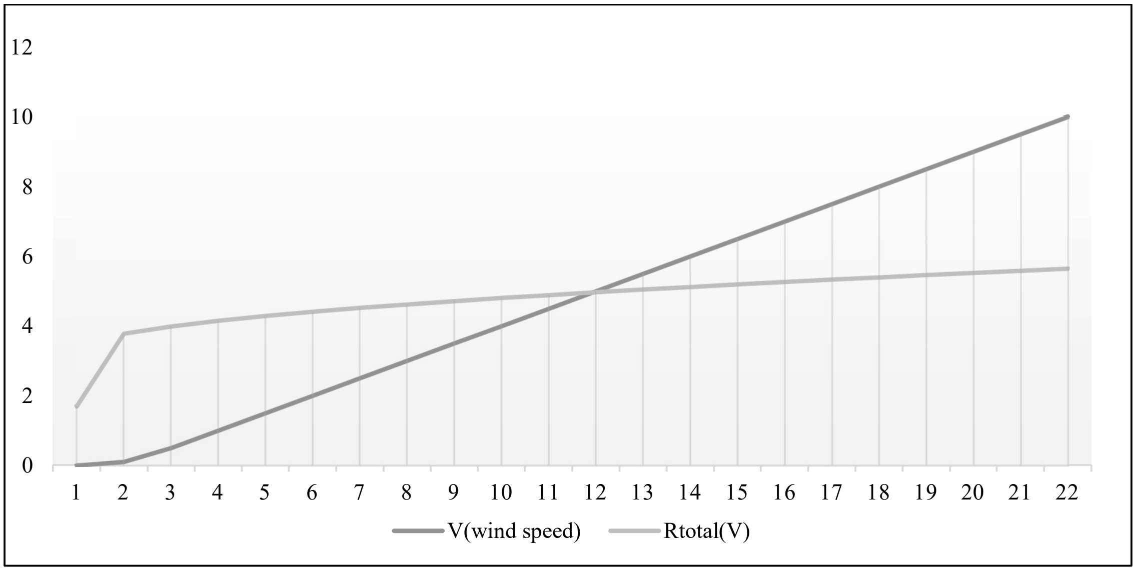

Figure 5. Illustration graph of the correlation of overall total thermal resistance of the hollow precast wall at difference input of wind speed ranging from 0.1 to 10 m/s.

The dataset shows a strong initial rise in thermal resistance with airflow. Between 0 and 0.1 m/s, resistance increases from 1.696 to 3.781 K/W (about 38%), indicating that even minimal airflow substantially disrupts boundary-layer formation. Beyond this, increases are gradual—3.985 K/W at 0.5 m/s, 4.156 K/W at 1 m/s, 4.969 K/W at 5 m/s, and 5.646 K/W at 10 m/s. This trend reflects the interaction between forced airflow and cavity dynamics, in which enhanced internal mixing alters temperature gradients and increases total resistance rather than simply providing convective cooling [7]. The behavior aligns with established patterns for transition from natural to forced convection in enclosed cavities [61]. As R_total rises, thermal equilibration slows, highlighting the importance of evaluating both transient and steady-state effects in ventilated wall design.

U-value behavior follows the same pattern. At 0 m/s, U = 0.590 W/m²K, dropping sharply to 0.265 W/m²K at 0.1 m/s (27.6% reduction). Later changes are smaller: 0.251 W/m²K at 0.5 m/s, 0.247 W/m²K at 1 m/s, 0.201 W/m²K at 5 m/s, and 0.178 W/m²K at 10 m/s. This diminishing sensitivity at higher speeds matches earlier findings that airflow becomes fully forced, limiting further gains [19]. Overall, the results show that low airflow (around 0.1 m/s) delivers the largest improvement in thermal performance, while increases beyond about 2–3 m/s yield only marginal benefits—useful guidance for low-energy or passive ventilation strategies.

Table 6. The point of difference thermal transmittance at each wind speed within building envelope

Wind speed (m/s)	U-Value ($W/m^2 \cdot K$)
0.0	0.590
0.1	0.265
0.5	0.251
1.0	0.241
1.5	0.233
2.0	0.227
2.5	0.221
3.0	0.216
3.5	0.212

Vol. 6, No. 2, pp. 170-193
Submit: 04-07-2025 |
Accepted: 29-12-2025 |
Publish: 31-12-2025 |

Wind speed (m/s)	U-Value (W/m^2·K)
4.0	0.208
4.5	0.205
5.0	0.201
5.5	0.198
6.0	0.195
6.5	0.193
7.0	0.190
7.5	0.188
8.0	0.185
8.5	0.183
9.0	0.181
9.5	0.179
10.0	0.177

3.3. Potential Application

The potential feature explored in the current system design is the reuse of exhaust air from the bathroom to drive ventilation within the hollow precast wall. This approach optimizes the building's internal airflow dynamics and contributes to thermal regulation within the building envelope, as shown in figure 4. In this configuration, air extracted from the bathroom, particularly from a lower level, is redirected to the base of the air cavity in the upper-level wall panel (e.g., in the bedroom). Because exhaust air is relatively cooler than the exterior daytime temperature, particularly in hot-humid climates, its entry into the cavity creates a temperature differential that enhances the stack effect. This supports natural convection by enabling cooler air to displace warmer air upward, facilitating efficient heat removal through the upper cavity outlets.

3.4. Energy Saving Analysis

This analysis evaluates the energy savings achieved by installing an air blower system around the perimeter of a 100-meter house to generate wind-assisted cooling at 0.1 m/s. The performance is compared against a no-wind condition, with all energy calculations based on electricity prices from the Board of Investment of Thailand (BOI) and the Electricity Generating Authority of Thailand (EGAT) [40].

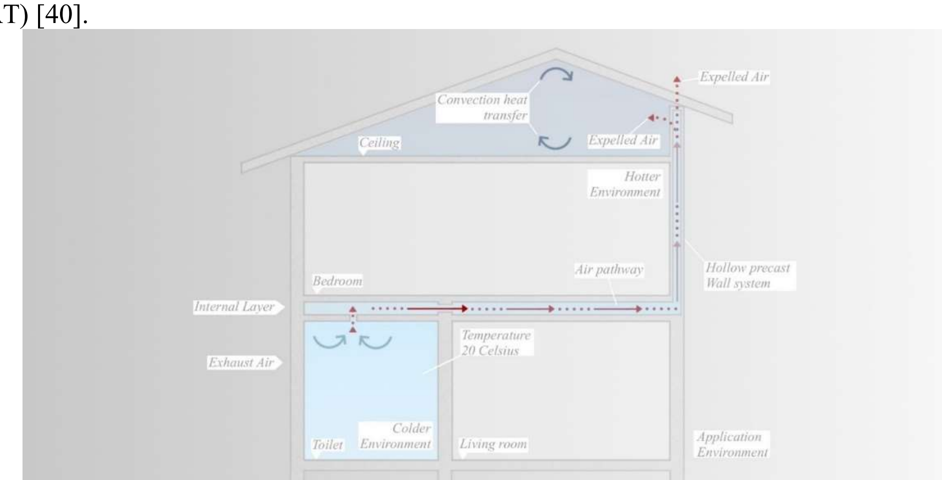

Figure 6. illustrates the proposed strategy for utilizing exhaust air from a lower-level toilet to drive ventilation within an hollow precast wall situated on the upper floor. This system leverages the temperature differential between the cooler exhaust air from the bathroom and the warmer external air to facilitate passive ventilation and enhance heat removal.

JICE Journal Innovation of Civil Engineering
Vol. 6, No. 2, pp. 170-193
Submit: 04-07-2025 |
Accepted: 29-12-2025 |
Publish: 31-12-2025 |

Where the equations that supporting case A and B cases are;

$$\mathrm{Q} = q \cdot L \tag{44}$$

Where Q is Heat transfer rate [W/m], q is heat transfer rate per unit length of wall [W/m], L is total perimeter length of wall [m].

$$\mathrm{E} = Q \cdot t \tag{45}$$

Where E is Annual cooling load [kWh/year], Q is Heat transfer rate [W/m], t is annual operating hours of daytime cooling [h/year].

$$E_b = P_b \cdot N_b \cdot t_b \tag{46}$$

Where E_b is Energy Consumption of Air Blowers [kWh/year], P_b is power of one blower [kW], N_b is number of blowers [equal to perimeter length in meters], t_b is annual blower operating hours [h/year].

$$E_{net} = E_{wind} + E_b \tag{47}$$

Where E_{net} is Net Annual Energy Usage with Wind Assistance [kWh/year], E_{wind} is annual cooling load with wind [kWh/year], E_b is annual blower energy [kWh/year].

$$\Delta E = E_{no\,wind} + E_{net} \tag{48}$$

Where ΔE is Energy Savings [kWh/year], $E_{no\,wind}$ is annual energy without wind [kWh/year], E_{net} is annual energy with wind + blower consumption [kWh/year]

$$\mathrm{C} = \Delta E \cdot p \tag{49}$$

Where C is financial saving [THB], ΔE is Energy Savings [kWh/year], p is electricity price [THB/kWh or USD/kWh depending on context] In the no-wind condition, the heat transfer rate is 2830.18 W/m, or 283.02 kW for a 100-m perimeter.

With 0.1 m/s wind assistance, the rate drops to 1269.62 W/m (126.96 kW). For annual operation, the cooling period assumes 5 minutes of blower use per hour over 8 hours daily, totaling 2,920 hours per year. Under these conditions, the wind-assisted system requires 370,891.20 kWh/year (126.96 kW × 2,920 h). Air delivery is supplied by 100 blowers (1-m spacing), each rated at 100 W, consuming 29,200 kWh/year (0.1 kW × 2,920 h × 100). Total energy use for the wind-assisted condition is therefore 400,091.20 kWh/year. Without wind assistance, annual energy use is 826,019.84 kWh/year (283.02 kW × 2,920 h). Thus, the annual energy savings equal 425,928.64 kWh/year. At the Thai electricity rate of 4.15 THB/kWh, savings reach 1,766,573.89 THB/year; using the U.S. average of 0.19 USD/kWh, the equivalent savings are 80,926.44 USD/year. These results demonstrate the substantial efficiency advantage of wind-assisted cooling for reducing energy consumption and operating costs [26].

The energy-saving results confirm that the hollow precast wall system is effective for improving thermal performance in hot climates. Wind-assisted cooling significantly reduces heat transfer, lowering cooling demand and supporting broader energy-efficiency and carbon-reduction goals. The air cavity functions as a thermal buffer, making the system suitable for passive and hybrid ventilation strategies. Controlled airflow enhances heat dissipation and enables adaptive responses to outdoor conditions, aligning with climate-responsive façade technologies. The system also offers

Vol. 6, No. 2, pp. 170-193
Submit: 04-07-2025 |
Accepted: 29-12-2025 |
Publish: 31-12-2025 |

potential for integration with underground cooling, where cooler subsurface air can be channeled through the cavity to provide geothermal-assisted passive cooling, similar to earth-air tunnel systems.

Design flexibility further strengthens its applicability: in high-rise façades, it can reduce heat absorption and contribute to urban heat-island mitigation, while in residential buildings, it can pair with smart ventilation controls to optimize comfort and energy use. Additional gains are possible when combined with shading or green-roof systems in tropical or desert climates. Limitations include the assumption of a uniform 0.1 m/s airflow, potential variations due to blower performance or construction tolerances, and the lack of long-term reliability and maintenance assessment. Because results rely on simulations, full-scale environmental testing is required to confirm performance.Future work should include field validation, investigation of phase-change materials within the cavity, and exploration of renewable-energy operation such as solar-powered blowers. These steps will help advance the hollow precast wall from a promising concept toward practical, scalable deployment.

4. Conclusion

This study assesses the Active Double-Layered Precast Wall Panel (ADLP) as a hybrid cooling system combining hollow precast insulation with low-speed ventilation. Introducing only 0.1 m/s airflow within the cavity reduces the U-value from 0.590 to 0.265 W/m²K (27.6%) and lowers heat transfer by 55.1%. Applied to a 100-meter perimeter house (625 m² wall area), the system delivers substantial annual cooling-load reductions. Although blowers installed at 1-meter intervals consume additional energy during their scheduled operation, the net yearly savings remain significant. The ADLP panel improves thermal performance by reducing cooling demand and enhancing envelope efficiency, making it suitable for hot, humid climates. Its modular design supports both new and retrofit applications, while integration with adaptive ventilation—such as underground cool-air channels or smart façades—can further enhance performance.

Results confirm hollow precast technology as a practical passive–hybrid cooling approach that reduces heat transfer, improves comfort, and lowers operating costs. At building scale, meaningful annual savings were achieved even after accounting for blower energy use. The study also provides a quantitative link between thermal modeling and performance evaluation. Limitations include reliance on simulation data and simplified airflow assumptions, underscoring the need for full-scale validation. Future research should optimize airflow strategies, evaluate renewable-powered or higher-efficiency blowers, and test enhancements such as phase-change materials or evaporative cooling to improve durability, cost-effectiveness, and applicability in low-energy building design.

References

[1] Abed, M. H., Al-Asadi, H. A., Samarmad, A. O., and Kadhim, S. A., "Improving building energy efficiency through ventilated hollow core slab systems. Case Studies in Thermal Engineering," vol. 60, p. 104793, 2024. doi: 10.1016/j.csite.2024.104793.
[2] B. Adhikary, A. Sahu, and P. Bhattacharya, "A coupled FE-RRM-based numerical model for analysis of energy transmission loss through stiffened double-wall panel due to TBL excitation," arXiv preprint arXiv:2208.11155, 2022. doi: 10.48550/arXiv.2208.11155.
[3] M. Ahsan-ul-Haq, S. Chand, M. Sajjad, and R. Usman, "Evaluating the suitability of two parametric wind speed distributions: A case study from Pakistan," Modeling Earth Syst. Environ., vol. 7, pp. 1–12, 2021. doi: 10.1007/s40808-020-00899-3.
[4] B. Akash, "Some prospects of energy savings in buildings," Energy Conversion and Management, vol. 42, no. 4, pp. 473–479, 2001. doi: 10.1016/S0196-8904(00)00140-0.
[5] A. Alaidroos and M. Krarti, "Optimized controls for ventilated wall cavities with spray evaporative cooling systems," Energy Build., vol. 154, pp. 356–372, 2017. doi: 10.1016/j.enbuild.2017.08.076.
[6] A. Aldersoni, A. Albaker, M. Alturki, and M. A. Said, "The Impact of Passive Strategies on the Overall Energy Performance of Traditional Houses in the Kingdom of Saudi Arabia," Buildings, vol. 12, no. 11, p. 1837, 2022. doi: 10.3390/buildings12111837.

Vol. 6, No. 2, pp. 170-193
Submit: 04-07-2025 |
Accepted: 29-12-2025 |
Publish: 31-12-2025 |

[7] N. Amar, N. Kishan, and B. S. Goud, "MHD heat transfer flow over a moving wedge with convective boundary conditions with the influence of viscous dissipation and internal heat generation/absorption," Heat Transfer, vol. 51, no. 5, pp. 5015–5029, 2022. doi: 10.1002/htj.22534.
[8] S. Pessiki and J. B. Lee, "Analytical investigation of thermal performance of precast concrete three-wythe sandwich wall panels," PCI J., vol. 49, pp. 88–101, 2004. doi: 10.15554/pcij.07012004.88.101.
[9] G. Bekdaş et al., "Prediction of Cooling Load of Tropical Buildings with Machine Learning," Sustainability, vol. 15, no. 11, p. 9061, 2023. doi: 10.3390/su15119061.
[10] J. G. Brida, D. Matesanz Gómez, and V. Segarra, "On the empirical relationship between tourism and economic growth," Tourism Manage., vol. 81, p. 104131, 2020. doi: 10.1016/j.tourman.2020.104131.
[11] A. Briga-Sá, J. Boaventura-Cunha, J. Lanzinha, and A. Paiva, "Experimental and analytical approach on the Trombe wall thermal performance parameters characterization," Energy Build., vol. 150, pp. 262–280, 2017. doi: 10.1016/j.enbuild.2017.06.018.
[12] L. Oliveira de Souza, H. A. Souza, and E. F. Rodrigues, "Experimental and numerical analysis of a naturally ventilated double-skin façade," Energy Build., vol. 165, 2018. doi: 10.1016/j.enbuild.2018.01.048.
[13] C. Chan, S. Y. Hu, M. Raynal, and Y. Leung, "A theoretical model on forced air movement in a divergent chimney for energy generation," in Proceedings of the 2013 International Conference on Applied Thermal Engineering, 2013, pp. 123–130.
[14] J. Chen, X. Xu, J. Zhou, and B. Li, "Interfacial thermal resistance: Past, present, and future," Rev. Mod. Phys., vol. 94, no. 2, p. 025002, 2022. doi: 10.1103/RevModPhys.94.025002.
[15] S.-E. Chorfi, G. El Guermai, M. Lahcen, and W. Zouhair, "Numerical identification of initial temperatures in heat equation with dynamic boundary conditions," Mediterr. J. Math., vol. 20, no. 4, pp. 1–22, 2023. doi: 10.1007/s00009-023-02461-8.
[16] R. Christopher and U. B., "Ventilated hollow core slab cooling load reduction under the operative temperature metric," IOP Conf. Ser.: Mater. Sci. Eng., vol. 609, no. 4, p. 042082, 2019. doi: 10.1088/1757-899X/609/4/042082.
[17] K. Çomaklı and B. Yüksel, "Optimum insulation thickness of external walls for energy saving," Appl. Therm. Eng., vol. 23, pp. 473–479, 2003. doi: 10.1016/S1359-4311(02)00209-0.
[18] H. Dicko, "A Dynamic Insulation Technique for Building Envelop by Using Microchannels," ASME J. Eng. For Sustainable Buildings Cities, vol. 4, 2023. doi: 10.1115/1.4063445.
[19] N. Dukhan, "Forced convection of nanofluids in metal foam: An essential review," Int. J. Therm. Sci., vol. 187, p. 108156, 2023. doi: 10.1016/j.ijthermalsci.2023.108156.
[20] P. Eneren, Y. T. Aksoy, and M. R. Vetrano, "Experiments on Single-Phase Nanofluid Heat Transfer Mechanisms in Microchannel Heat Sinks: A Review," Energies, vol. 15, no. 7, p. 2525, 2022. doi: 10.3390/en15072525.
[21] J. Fourier, "Théorie analytique de la chaleur," University of Lausanne, 1822.
[22] T. Friedrich and R. Klein-Holte, "Flexurally Rigid Support of Prestressed Hollow Core Slabs with Post-tensioned Beams," in High Tech Concrete: Where Technology and Engineering Meet, Springer International Publishing, 2017. doi: 10.1007/978-3-319-59471-2_132.
[23] J. Han, L. Lu, and H. Yang, "Numerical evaluation of the mixed convective heat transfer in a double-pane window integrated with see-through a-Si PV cells with low-e coatings," Appl. Energy, vol. 87, pp. 3431–3437, 2010. doi: 10.1016/j.apenergy.2010.05.025.
[24] Y. Han, K. Ruan, and J. Gu, "Janus (BNNS/ANF)-(AgNWs/ANF) thermal conductivity composite films with superior electromagnetic interference shielding and Joule heating performances," Nano Res., vol. 15, 2022. doi: 10.1007/s12274-022-4159-z.
[25] Y.-L. He, K. Sun, Y. Wu, H.-S. Zhao, X.-L. Wang, C. Gerada, and D. Gerada, "Impact of Static Air-Gap Eccentricity on Thermal Responses of Stator Winding Insulation in Synchronous Generators," IEEE Trans. Ind. Electron., vol. 69, no. 12, pp. 13544–13554, 2022. doi: 10.1109/TIE.2021.3135627.

Vol. 6, No. 2, pp. 170-193
Submit: 04-07-2025 |
Accepted: 29-12-2025 |
Publish: 31-12-2025 |

[26] A. Hnatov, A. Patlins, S. Arhun, N. Kunicina, H. Hnatova, O. Ulianets, and A. Romanovs, "Development of an unified energy-efficient system for urban transport," in 2020 IEEE Energy Conversion Congress and Exposition (ECCE), 2020, pp. 248–253. doi: 10.1109/ENERGYCon48941.2020.9236606.

[27] H. H. Hosamo, H. K. Nielsen, D. Kraniotis, P. R. Svennevig, and K. Svidt, "Improving building occupant comfort through a digital twin approach: A Bayesian network model and predictive maintenance method," Energy Build., vol. 288, p. 112992, 2023. doi: 10.1016/j.enbuild.2023.112992.

[28] J. R. Howell, M. P. Mengüc, K. Daun, and R. Siegel, Thermal Radiation Heat Transfer, 7th ed., CRC Press, 2020. doi: 10.1201/9780429327308.

[29] J. Huang, J. Yu, and H. Yang, "Effects of key factors on the heat insulation performance of a hollow block ventilated wall," Appl. Energy, vol. 232, pp. 409–423, 2018. doi: 10.1016/j.apenergy.2018.01.048.

[30] I. Nardi, S. Perilli, T. de Rubeis, S. Sfarra, and D. Ambrosini, "Influence of insulation defects on the thermal performance of walls. An experimental and numerical investigation," J. Build. Eng., vol. 21, pp. 355–365, 2019. doi: 10.1016/j.jobe.2018.10.029.

[31] Iwaro, J., Mwasha, A., and Ramsubhag, K., "The Impact of Roof Thermal Performance on the Indoor Thermal Comfort in a Natural Ventilated Building Envelope in Hot Climatic Climates," Int. J. Civ. Environ. Eng., vol. 4, 2017.

[32] H. K. Jalghaf, E. Kovács, and B. Bolló, "Comparison of Old and New Stable Explicit Methods for Heat Conduction, Convection, and Radiation in an Insulated Wall with Thermal Bridging," Buildings, vol. 12, no. 9, p. 1365, 2022. doi: 10.3390/buildings12091365.

[33] G. Jasion et al., "0.174 dB/km hollow core Double Nested Antiresonant Nodeless Fiber (DNANF)," in Optical Fiber Communication Conference (OFC) 2022, 2022. doi: 10.1364/OFC.2022.Th4C.7.

[34] A. Karanafti, T. Theodosiou, and K. Tsikaloudaki, "Assessment of buildings' dynamic thermal insulation technologies-A review," Appl. Energy, vol. 305, p. 117985, 2022. doi: 10.1016/j.apenergy.2022.119985.

[35] J. S. Kay and S. Malik, "Impact of Improper Installation, Maintenance and Servicing of Electrical Equipment in Forest Products Industries," IEEE Trans. Ind. Appl., vol. PP, pp. 1–1, 2020. doi: 10.1109/TIA.2020.2987276.

[36] S. K. Kim, "Darcy friction factor and Nusselt number in laminar tube flow of Carreau fluid," Rheologica Acta, vol. 61, pp. 1–13, 2022. doi: 10.1007/s00397-021-01317-w.

[37] R. A. Kishore, C. Booten, and M. V. A. Bianchi, "Techno-Economic Analysis of Dynamic Building Envelopes Comprising Phase Change Materials and Switchable Insulations," NREL/CP-5500-82623, 2022.

[38] M. W. Liddament, Air infiltration calculation techniques: An applications guide, Air Infiltration and Ventilation Centre, 1986.

[39] L. Liu, Z. Yu, and H. Zhang, "Simulation study of an innovative ventilated facade utilizing indoor exhaust air," Energy Procedia, vol. 121, pp. 126–133, 2017. doi: 10.1016/j.egypro.2017.08.009.

[40] D. Liu, X. Liu, K. Guo, Q. Ji, and Y. Chang, "Spillover Effects among Electricity Prices, Traditional Energy Prices and Carbon Market under Climate Risk," Int. J. Environ. Res. Public Health, vol. 20, no. 2, p. 1116, 2022. doi: 10.3390/ijerph20021116.

[41] J. Liu, F. Tavakoli, S. M. Sajadi, M. Z. Mahmoud, B. Heidarshenas, and H. Ş. Aybar, "Numerical evaluation and artificial neural network modeling of the effect of oval PCM compartment dimensions around a triple lithium-ion battery pack despite forced airflow," Eng. Anal. Bound. Elem., vol. 142, pp. 71–92, 2022. doi: 10.1016/j.enganabound.2022.05.006.

[42] S. Ma, D. Hou, P. Bao, and D. Wang, "Influence of alkali-resistant glass fiber on seismic performance of precast ceramsite concrete sandwich wall panels," Structures, vol. 38, pp. 94–107, 2022. doi: 10.1016/j.istruc.2022.01.081.

Vol. 6, No. 2, pp. 170-193
Submit: 04-07-2025 |
Accepted: 29-12-2025 |
Publish: 31-12-2025 |

[43] T. M. I. Mahlia, T. Nur, I. Ismail, and H. H. Masjuki, "Correlation between thermal conductivity and the thickness of selected insulation materials for building wall," Energy and Buildings, vol. 39, no. 2, pp. 182–187, 2007. doi: 10.1016/j.enbuild.2006.06.002.

[44] B. S. Mahmood et al., "Alternating Directions Implicit Method for Solving Homogeneous Heat Diffusion Equation," Ibn AL-Haitham J. Pure Appl. Sci., vol. 33, no. 2, pp. 62–71, 2020. doi: 10.30526/33.2.2427.

[45] A. Marani and M. Madhkhan, "Thermal performance of concrete sandwich panels incorporating phase change materials: An experimental study," J. Mater. Res. Technol., vol. 12, pp. 760–775, 2021. doi: 10.1016/j.jmrt.2021.03.022.

[46] G. Marom, S. Grossbard, M. Bodek, E. Neuman, and D. Elad, "Computational analysis of a new biomimetic active ventilation paradigm for indoor spaces," Int. J. Numer. Methods Heat Fluid Flow, vol. 33, no. 8, pp. 2710–2729, 2023. doi: 10.1108/HFF-12-2022-0698.

[47] D. Meiramov, Y. Seo, H. Ju, and H.-C. Cho, "Direct Tensile Capacity of Steel-Tube Connections in a Precast Concrete Double-Wall System," Buildings, vol. 13, no. 11, p. 2872, 2023. doi: 10.3390/buildings13112872.

[48] F. Ochs, W. Heidemann, and H. Müller-Steinhagen, "Effective thermal conductivity of moistened insulation materials as a function of temperature," Int. J. Heat Mass Transf., vol. 51, pp. 539–552, 2008. doi: 10.1016/j.ijheatmasstransfer.2007.05.005.

[49] R. Pace, F. Chiocchini, M. Sarti, T. A. Endreny, C. Calfapietra, and C. Ciolfi, "Integrating Copernicus land cover data into the i-Tree Cool Air model to evaluate and map urban heat mitigation by tree cover," Urban Ecosyst., vol. 25, no. 6, p. 2125833, 2022. doi: 10.1080/22797254.2022.2125833.

[50] M. Proença, M. Garrido, J. R. Correia, and M. G. Gomes, "Fire resistance behaviour of GFRP-polyurethane composite sandwich panels for building floors," Compos. Part B Eng., vol. 224, p. 109171, 2021. doi: 10.1016/j.compositesb.2021.109171.

[51] S. Sumaya, D. Goyal, S. Keshari, F. Arslan, and B. Dugbakie, "Secure Wireless Networks Based on Fuzzy Logic for Smart HVAC Systems in Small-Scale Industries," Security Commun. Networks, vol. 2022, Article ID 3659961, 2022. doi: 10.1155/2022/3659961.

[52] M. S. Shadloo, "Application of support vector machines for accurate prediction of convection heat transfer coefficient of nanofluids through circular pipes," Int. J. Numer. Methods Heat Fluid Flow, ahead-of-print, 2020. doi: 10.1108/HFF-09-2020-0555.

[53] R. Ryan and S. Murray, "The combined effects of thermal mass and insulation on energy performance in concrete office buildings," Adv. Building Energy Res., vol. 14, pp. 1–16, 2019. doi: 10.1080/17512549.2018.1547220.

[54] N. Szemiot, A. Hoła, and Ł. Sadowski, "Assessment of the effectiveness of secondary anti-damp insulation in heritage buildings made of historic brick: the current state of knowledge, research gaps and perspectives," Herit Sci, vol. 11, p. 198, 2023. doi: 10.1186/s40494-023-01043-x.

[55] M. Vahabzadeh, A. Afshar, and A. Molajou, "Energy simulation modeling for water-energy-food nexus system: a systematic review," Environ. Sci. Pollut. Res., vol. 30, no. 3, pp. 5487–5501, 2023. doi: 10.1007/s11356-022-24300-1.

[56] J. B. Wang, Q. Z. Du, C. Zhang, X. H. Xu, and W. J. Gang, "Mechanism and preliminary performance analysis of exhaust air insulation for building envelope wall," Energy Build., vol. 173, pp. 516–529, 2018. doi: 10.1016/j.enbuild.2018.05.045.

[57] C. Wang, S. Holmberg, and S. Sadrizadeh, "Numerical study of temperature-controlled airflow in comparison with turbulent mixing and laminar airflow for operating room ventilation," Build. Environ., vol. 144, pp. 45–56, 2018. doi: 10.1016/j.buildenv.2018.08.010.

[58] J. Wang, Z. Huang, Y. Xu, and D. Xie, "Gas–Liquid Two-Phase Flow Measurement Based on Optical Flow Method with Machine Learning Optimization Model," Appl. Sci., vol. 14, no. 9, p. 3717, 2024. doi: 10.3390/app14093717.

[59] H. Xi, Q. Zhang, Z. Ren, G. Li, and Y. Chen, "Urban Building Energy Modeling with Parameterized Geometry and Detailed Thermal Zones for Complex Building Types," Buildings, vol. 13, no. 11, p. 2675, 2023. doi: 10.3390/buildings13112675.

Vol. 6, No. 2, pp. 170-193
Submit: 04-07-2025 |
Accepted: 29-12-2025 |
Publish: 31-12-2025 |

[60] S. Xia, "Heat engine cycle configurations for maximum work output with generalized models of reservoir thermal capacity and heat resistance," J. Non-Equilib. Thermodyn., vol. 47, no. 3, pp. 503–517, 2022. doi: 10.1515/jnet-2022-0029.

[61] G. Yao, Y. Chen, Y. Yang, Y. Zheng, L. Wu, and H. Du, "Research on Mechanism of Vortex-Induced Vibration Railing Effect of Double-Deck Large-Span Suspension Bridge," Appl. Sci., vol. 13, no. 16, p. 9314, 2023. doi: 10.3390/app13169314.

[62] T. Zhang, Y. Tan, H. Yang, and X. Zhang, "The application of air layers in building envelopes: A review," Appl. Energy, vol. 165, pp. 707–734, 2016. doi: 10.1016/j.apenergy.2015.12.108.

[63] N. Zhangabay, I. Baidilla, A. Tagybayev, and B. Sultan, "Analysis of Thermal Resistance of Developed Energy-Saving External Enclosing Structures with Air Gaps and Horizontal Channels," Buildings, vol. 13, no. 2, p. 356, 2023. doi: 10.3390/buildings13020356.

[64] L. Zhu, L. Tian, S. Jiang, L. Han, Y. Liang, Q. Li, and S. Chen, "Advances in photothermal regulation strategies: from efficient solar heating to daytime passive cooling," Chem. Soc. Rev., vol. 52, no. 21, pp. 7068–7090, 2023. doi: 10.1039/D3CS00057J.

[65] K. Phaiboonnukulkij, “Interlocking passive brick set: the design of interlocking building components with connecting air cavities for heat dissipation and as a complement to the Heating, Ventilation, and Air Conditioning (HVAC) system”, *Bud-Arch*, vol. 23, no. 4, pp. 091–111, Dec. 2024.